

Numerical evaluation of the influence of compaction and soil strength parameters on GRSW

Leone César Meireles¹ , Mario Vicente Riccio Filho² , Heraldo Nunes Pitanga² ,
Roberto Lopes Ferraz³ , Taciano Oliveira da Silva³ ,
Sérgio Leandro Scher Dias Neto^{3#} 

Article

Keywords

Numerical modelling
Compaction
Deformations
Reinforced soils

Abstract

This paper presents a numerical evaluation, using PLAXIS 2D finite element software, of the effects of varying the distance of the heavy compaction from the face in a geosynthetic reinforced soil wall (GRSW). The main effects studied were the tensions in the reinforcements and the horizontal deformations of the face, including the influence of the type of shear strength envelope (total stresses or effective stresses) of the soil. In this study, a young gneiss residual soil (silty sand) was studied to obtain the grain size distribution, index properties and parameters of strength and deformability. This soil was considered for backfill in hypothetical sections of GRSW. The numerical results contributed to a better understanding of the GRSW behaviour, with evaluations closer to real field conditions. In the analyses carried out, when increasing the heavy compaction distance from the face, there are tendencies pointing to the reduction of the tensions in the reinforcements, displacement toward the interior of the soil mass of the points at which the maximum reinforcement tension occurs and reduction of the horizontal deformations of the face.

Introduction

In geosynthetic reinforced soil walls (GRSW), several factors influence the distribution of tensions and deformations in the reinforced soil mass, such as the wall height, stiffness and spacing of reinforcements, stiffness and slope of the face, foundation conditions, backfill soil characteristics, effect of tensions induced by compaction, application of overloads and restriction to the displacements of the base, etc. In recent decades, several authors have developed studies based on experimental and/or numerical evaluations to determine the effects of these influencing factors on the mechanical behaviour of GRSW [e.g., Bathurst & Ezzein (2016), Chen et al. (2017), Ehrlich et al. (2012), Ehrlich & Mirmoradi (2013), Hatami & Bathurst (2005), Mirmoradi et al. (2016), Mirmoradi & Ehrlich (2018a, b), Riccio et al. (2014), Saramago (2002)].

As highlighted by Mirmoradi (2015), despite the several studies carried out, the results indicate that there is a need for additional studies to better understand the effects of the influencing factors for predicting the maximum traction mobilized in the reinforcement elements (T_{max}), the main factor to be determined for adequately designing GRSW (Ehrlich

& Mirmoradi, 2016) and predicting face displacements and traction in reinforcements.

Several studies present a constructive recommendation that a backfill soil strip close to the face should be compacted with less energy to reduce the horizontal tensions close to the face and, consequently, the deformations due to the construction process [e.g., Bathurst et al. (2009), Ehrlich & Mitchell (1994), Elias et al. (2001), Hatami et al. (2008), Koerner & Koerner (2018), Mirmoradi & Ehrlich (2018b), Mitchell & Villter (1987)]. Although this recommendation is widely found in the literature, this factor has rarely been considered in the developed studies, as emphasized by Mirmoradi & Ehrlich (2018a).

In the present study, aiming to contribute to understanding the mechanical behaviour of the GRSW, with approaches increasingly closer to the real field conditions, the effects of the distance of application of heavy compaction from the face of GRSW were analysed numerically in terms of tensions and deformations. From a typical section, the analyses were performed with variations in the stiffness of the reinforcements and the distances of heavy compaction application from the face (light and heavy compaction were considered). In addition, for the backfill soil, after characterization and laboratory tests,

Corresponding author. E-mail address: sergio.neto@ufv.br

¹ Samarco Mineração, Belo Horizonte, MG, Brasil.

² Universidade Federal de Juiz de Fora, Faculdade de Engenharia, Juiz de Fora, MG, Brasil.

³ Universidade Federal de Viçosa, Departamento de Engenharia Civil, Viçosa, MG, Brasil.

Submitted on March 6, 2022; Final Acceptance on October 4, 2022; Discussion open until February 28, 2023.

<https://doi.org/10.28927/SR.2022.003022>



This is an Open Access article distributed under the terms of the Creative Commons Attribution License, which permits unrestricted use, distribution, and reproduction in any medium, provided the original work is properly cited.

the strength parameters in terms of total and effective stresses were considered (triaxial strength envelopes). A comparison between the results is presented, considering the position and magnitude of the maximum tension mobilized in the reinforcements (T_{max}) and the horizontal displacements of the face at the end of the construction period.

1. Material and methods

1.1. Typical analysis section

For the numerical analyses in terms of tensions and deformations, a typical hypothetical GRSW retaining structure with a typical configuration adopted in several works was considered. The studied hypothetical structure was composed of precast concrete blocks and used geogrids as a geosynthetic reinforcement element and a gravel layer for drainage, just behind the face blocks. Table 1 lists the main geometric characteristics of the analysis section shown in Figure 1.

The numerical analyses were performed using the finite element method in PLAXIS 2D (Brinkgreve & Vermeer, 2002) with consideration of the plane strain state. In Figure 2 the boundary conditions adopted can be observed, namely, the restriction of horizontal displacement on the sides of the section—on the left side only applied to the foundation—and

the total restriction of displacements and rotation at the base. The typical section was discretized in triangular elements composed of 15 nodes. The overall refinement adopted for the mesh was classified as Medium and, close to the contacts with reinforcements and the face, Very Fine. The mesh has a total of 3,007 elements and 24,299 nodes.

1.2. Material properties

The linear elastic constitutive model was used for the face blocks. The parameters were defined according to the experimental results obtained by Mohamad et al. (2007). The soil-block interface friction factor (R_{inter}) was set as 0.7 (i.e., $\mu = 0.7 \cdot \tan \phi'$), where ϕ' is the effective friction angle of the soil backfill. For the drainage layer, the work of Riccio et al. (2014) was used, in which the material is presented with the Hardening Soil constitutive model similar to the hyperbolic fit proposed by Duncan et al. (1980), which considers the variation in the elastic modulus in relation to the confining stress (σ_3), in addition to considering the effect of soil dilatancy and introducing a plastification function. In the model, the plastification surface is not fixed in the stress space but expands due to plastic deformations (Brinkgreve & Vermeer, 2002). For the drainage layer, the standard recommendation of the PLAXIS 2D software was used, with $E_{ur}^{ref} = 3E_{50}^{ref}$, in which E_{ur}^{ref} and E_{50}^{ref} are the stiffnesses of the material for the reference confining tension (p^{ref}), corresponding to 50% of the maximum deformation, respectively, in unloading and loading. In addition, the software considers the tangent modulus obtained from oedometric tests (E_{eod}^{ref}) and the exponential coefficient (m) applied in the relationship between stiffness and tension level. In the present study, the adopted value of E_{eod}^{ref} was equal to the value of E_{50}^{ref} , which is the value obtained from the triaxial tests for an effective consolidation stress of 80 kPa. The value of m was also obtained from the stress-deformation curves of

Table 1. Main geometric characteristics of the analysis section.

Description	Value
Free height (m)	4.20
Face inlay (m)	0.40
Face inclination	1H:10V
Length of reinforcements (m)	3.50
Vertical spacing between reinforcements (m)	0.40

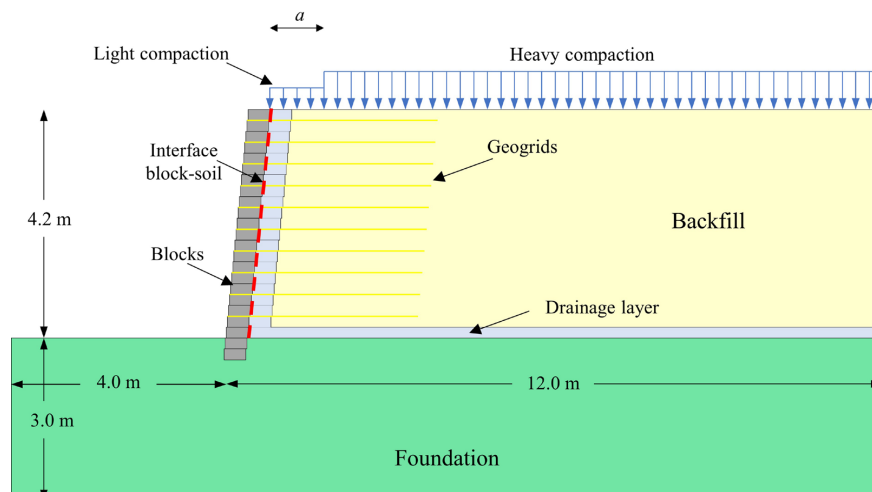


Figure 1. Analysed section with variations of the external loading.

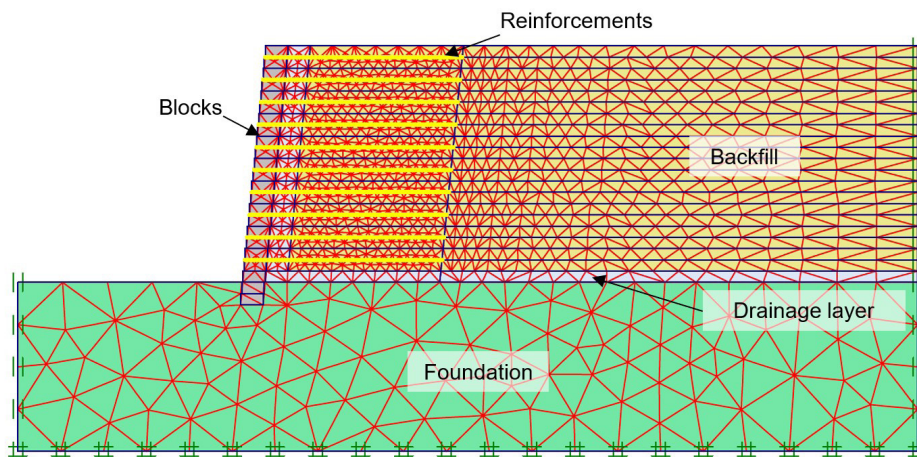


Figure 2. Numerical model and finite element mesh in PLAXIS 2D.

Table 2. Soil characteristics.

$\phi^* \leq 2 \mu\text{m}$ (%)	$\phi \leq 20 \mu\text{m}$ (%)	$\phi \leq 2 \text{mm}$ (%)	w_{opt} (%)	$\gamma_{d,max}$ (kN/m ³)
10	22	100	13.8	17.43

* ϕ : effective diameter of soil particles.

the triaxial tests for effective consolidation stresses (σ_3) of 40, 80, 160 and 320 kPa.

The elastoplastic constitutive model, with the Mohr-Coulomb failure criterion, was considered for the foundation. The parameters of the foundation were assigned in such a way that it had a good bearing capacity and did not significantly influence the values of maximum tensile stresses acting on the reinforcements.

The backfill soil adopted in the analyses, a young gneiss residual soil, was characterized in the laboratory. On specimens moulded to a 98% degree of compaction at Normal Proctor energy, hydrostatic and undrained triaxial tests were performed in the saturated condition (CIU_{sat}), according to D4767 (ASTM, 2011), using consolidation stresses (σ_3) of 40, 80, 160 and 320 kPa. Table 2 presents the values obtained in the characterization and Normal Proctor tests for the studied soil.

The soil backfill was modelled with the Hardening Soil constitutive model, using the approach explained earlier for the drainage layer. The parameters for the hyperbolic relationship between stress and strain were defined to obtain the best fit of the hyperbole to the curves obtained in the triaxial tests.

For the test carried out with an effective consolidation stress of 320 kPa, an unloading and reloading cycle was performed. In this way, the real ratio between the reload stiffness and the initial stiffness (E_{ur}/E_i) was obtained. In general, using the real ratio (E_{ur}/E_i) is rarely considered. The parameters of the mentioned materials are listed in Table 3. As the backfill soil was submitted to loading and unloading due to compaction, determining the E_{ur}/E_i ratio is relevant.

The reinforcement elements were modelled as a linear elastic material using the hypothesis of perfect adherence with adjacent soil. Under working conditions, this hypothesis is considered acceptable, as presented by Jewell (1980) and Dyer & Milligan (1984). Geogrids were considered for the geosynthetic reinforcements, which are made up of polyester (PET) polymers whose stiffnesses are as follows: R1 = 400 kN/m, R2 = 800 kN/m and R3 = 1500 kN/m. Stiffness values were selected for 5% deformation.

1.3. Compaction

The calculation of the vertical stress induced by compaction (σ_{zci}) was performed using the procedure proposed by Ehrlich & Mitchell (1994). Two compaction devices were considered, namely a heavy compactor (compactor roller) and a light compactor (vibratory plate). A typical vibratory plate had a vertical induced stress measured by Saramago (2002) using accelerometers. The measurements show a vertical stress induced by the equipment of approximately 73 kPa. The compactor roller (type CA 250 PD, Dynapac), as presented by Riccio et al. (2014), presents a maximum vertical force (Q) of 378 kPa. For the calculation of σ_{zci} by the procedure proposed by Ehrlich & Mitchell (1994), the friction angle of the backfill soil and characteristics of the compaction equipment were used. Stresses induced by compaction were evaluated using parameters obtained from the shear failure envelopes in terms of total and effective stresses.

The Type 2 procedure proposed by Mirmoradi & Ehrlich (2014) was adopted for compaction simulation in

Table 3. Input parameters adopted in the numerical modelling for the drainage layer, the face blocks and the foundation soil of the typical sections analysed.

Materials	Backfill soil*		Drainage layer	Blocks	Foundation
Constitutive Model	<i>Hardening Soil Model</i>		<i>Hardening Soil Model</i>	<i>Linear elastic</i>	<i>Elastoplastic with Mohr-Coulomb failure criterion</i>
Stress path	Total	Effective	-	-	-
Friction angle, ϕ (°)	60	36	40	-	35
Cohesion (kPa)	20	6	0	-	10
Dilatancy angle, ψ (°)	2	2	0	-	0
Unit weight, γ (kN/m ³)	20	19	20	25	20
E_{50}^{ref} (MPa)	9	9	40	-	-
E_{oed}^{ref} (MPa)	9	9	55	-	-
E_{ur}^{ref} (MPa)	22	22	120	-	-
Exponent modulus, m	0.7	0.7	0.5	-	-
Young modulus, E (MPa)	-	-	-	50	50
Poisson Coefficient, ν	0.3	0.3	-	0.2	0.3

*The backfill soil parameters are listed in detail in item 3.1.

the numerical analyses. In this procedure, the compaction of each layer is simulated by a single load-unload cycle, with the application of the vertical stress induced by compaction ($\sigma_{zc,i}$) at the top and bottom of the layer. The authors found that the Type 2 procedure represents, more appropriately, the efforts due to compaction.

1.4. Numerical analysis program

Table 4 shows the analysis program corresponding to the simulations carried out and the corresponding codes assigned to them. For the analysis section presented previously (Figure 1), analyses were performed in terms of effective stress (ES) and total stress (TS) for reinforced soil using three (03) types of reinforcement and four (04) distances of heavy compaction from the face (a). The distances considered are 0, 0.25, 0.5 and 1.0 m.

2. Results and discussions

2.1. Laboratory tests

The laboratory characterization of the backfill soil indicates that it has a unified classification, according to D2487 (ASTM, 2017), SM (Silty sand). The use of fine-grained soils for GRSW is a common practice in Brazil, an example is given in Riccio et al. (2014).

Figure 3 shows a compilation of the results of the hydrostatic and consolidated undrained triaxial tests in the saturated condition (CIU_{sat}). As can be seen in Figure 3a, the material presented an increase in its Young's modulus with increasing confining stress (σ_3), that is, the higher is the confining stress (σ_3) the higher the Young's modulus (E).

From the stress-strain curves, the parameters of the hyperbolic fit (Duncan et al., 1980) were optimized to obtain the best fit for determining parameters K and m . Figure 3a shows the hyperbolic fit each stress-strain curve ($\sigma_3 = 40, 80, 160$ and 320 kPa) obtained from the triaxial tests. A better fit in the initial stretches of the curves was chosen since the GRS walls have small horizontal deformations.

Figure 3b shows the envelopes for trajectories of total and effective stresses. The strength parameters, cohesion intercept (c or c') and friction angle (ϕ or ϕ') were determined from the envelopes (solid lines) obtained from the maximum value of σ_d (deviator stress) of each experimental stress-strain curve. Thus, the effective strength parameters were $c' = 6$ kPa and $\phi' = 36^\circ$, and the total strength parameters were $c = 60$ kPa and $\phi = 20^\circ$. This difference between the parameters obtained from the total and effective stress envelopes leads to significant differences in the prediction of the tension in the reinforcements.

Figure 3c illustrates the unload-reload cycle carried out in the test with a 320 kPa effective consolidation stress. A 149.55 MPa stiffness (E_{ur}) was obtained. Since the initial stiffness (E_i) obtained was 61.7 MPa for the test with the same effective consolidation stress, the real E_{ur} / E_i ratio obtained was 2.4. It should be noted that this value is within the typical range presented by Duncan et al. (1980).

2.2. Magnitude of maximum tension in the reinforcements (T_{max})

Figure 4 presents a compilation of the results of maximum tension in the reinforcements (T_{max}) obtained in the numerical analyses that provided data to evaluate the influence of the distance of heavy compaction from the face. For a better understanding of these results, the sum of

Table 4. Data corresponding to the analyses carried out and the code for each.

Shear failure envelope	Reinforcement	a (cm)	Distance of Heavy compaction from the face	Code
Effective stress (ES)	R1 (J = 400 kN/m)	0		ES-R1-0
		25		ES-R1-25
		50		ES-R1-50
		100		ES-R1-100
	R2 (J = 800 kN/m)	0		ES-R2-0
		25		ES-R2-25
		50		ES-R2-50
		100		ES-R2-100
	R3 (J = 1500 kN/m)	0		ES-R3-0
		25		ES-R3-25
		50		ES-R3-50
		100		ES-R3-100
Total stress (TS)	R1 (J = 400 kN/m)	0		TS-R1-0
		25		TS-R1-25
		50		TS-R1-50
		100		TS-R1-100
	R2 (J = 800 kN/m)	0		TS-R2-0
		25		TS-R2-25
		50		TS-R2-50
		100		TS-R2-100
	R3 (J = 1500 kN/m)	0		TS-R3-0
		25		TS-R3-25
		50		TS-R3-50
		100		TS-R3-100

the maximum tensions acting on the reinforcements (ΣT_{max}) and the sum of the positions at which the maximum tensions (ΣX_{max}) occur were plotted in the graphs, in which X is the distance from the point at which the maximum took place far from the back side of the face.

In general, when distancing the heavy compaction from the face, there are reductions in the maximum tensions mobilized in the reinforcements and displacement of the points at which they occur to the interior of the reinforced soil mass.

For the analyses considering effective parameters for the backfill soil (Figure 4a, b and c), average reductions of ΣT_{max} (3, 7 and 12%) were obtained when considering, respectively, the distances of heavy compaction of 0.25, 0.50 and 1.0 m from the face. On the other hand, when considering the sum of the positions of points at which maximum tensions occur (ΣX_{max}), there was, respectively, an increase in the sum of the positions where T_{max} occurs by 4, 9 and 36%; that is when increasing the distance of heavy compaction from the face, the point where T_{max} occurs moves to the interior of the soil mass.

For the analyses in which the total parameters for the backfill soil were considered (Figure 4d, e and f), there is a smaller influence of the distance of heavy compaction from the face on the comparison parameters (ΣT_{max} and ΣX_{max}). The sum of the maximal tensions in the reinforcements

(ΣT_{max}) showed reductions of 1, 2 and 4% when considering, respectively, the distances of heavy compaction from of 0.25, 0.50 and 1.0 m the face. When considering the sum of the position of points where the maximum tension occurs (ΣX_{max}), the average positions move towards to the interior of the soil mass, increasing, respectively, by 1, 4 and 5%.

It is important to point out that, for the analyses considering of total parameters of the backfill soil, as already mentioned, due to the reduction in the friction angle ($\phi' = 36^\circ$ to $\phi = 20^\circ$), there is a reduction in the vertical stress induced by compaction, which is 80 kPa. The vertical stress induced by the light compaction applied close to the face is 73 kPa, independent of the soil friction (compaction per hand tamper, $\sigma'_{z,i} = F/A$, F is the static equivalent weight and A is the area of the plate).

Regardless of kind of strength parameters (effective or total), the behaviour observed is the following, the higher distance of heavy compaction from the face, the lower the ΣT_{max} and the sum of the distance between the location of the T_{max} and the face increase.

Regarding the stiffness of geosynthetic reinforcements (Figure 4), in the analyses based on effective parameters (ES analyses) and in the analyses based on total parameters (TS analyses), the values of the maximum tensions in the reinforcements increase with the increase in the stiffness modulus of the geosynthetic reinforcement.

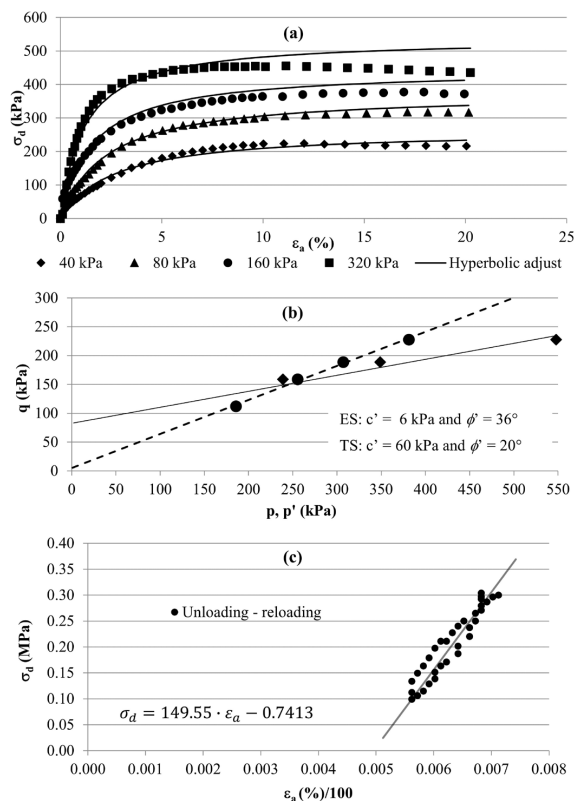


Figure 3. Results from the CIUsat triaxial tests for σ_3 equal to 320 kPa, considering the unload-reload cycle - (a) deviator stress (σ_d) versus axial strain (ϵ_a) curves, (b) failure envelopes in terms of total stress (TS) and effective stress (ES) and (c) unload-reload cycle.

2.3. Position of the maximum tension in the reinforcements (X_{max})

Figure 5 and Figure 6 illustrate the points at which the maximum tensions mobilized in the reinforcements (X_{max}) occur for the analyses performed with effective and total backfill soil parameters, respectively.

The stiffness variation of the reinforcements did not result in significant differences in the points at which the maximum tensions occur. For the two upper layers of the reinforcements, taking into account the effective parameters of the backfill soil, the displacement of the points of maximum tensions towards the interior of the soil mass with increasing distance of the application of heavy compaction from the face. This behaviour is associated with the fact that the vertical induced stress due compaction is much higher than the geostatic vertical stress. The vertical induced stress produce a horizontal induced stress ($\sigma'_{xp,i} = K_o \cdot \sigma'_{zc,i}$) loading the reinforcement. Thus, the location of T_{max} has a tendency to move towards the region where the compaction was applied, moving away from the proximity of the face, where there is no compaction. This displacement is shown to be important for evaluating the stability to pulling out the reinforcement element. For the analyses with the use of total parameters of

the backfill soil (Figure 6), as mentioned for T_{max} results, due to the small difference between heavy and light compaction, the results are very similar.

Concerning the points of maximum tension in the reinforcements, it is emphasized that because it is a GRSW with a rigid face, there is a tendency for these points to occur close to the face (Christopher et al., 1990).

The displacement of the point of maximum tension to the interior of the soil mass implies an increase in the length of the reinforcement in the active zone of the reinforced soil and, consequently, a reduction in the length in the resistant zone, which causes reduction of the factor of safety to the pull-out of the element (Chen et al., 2017).

2.4. Horizontal displacements of the face

A comparison was made between the results obtained for the horizontal displacements (U_x) of the face, considering the analyses performed using effective and total shear strength parameters. In general, the results are consistent with reinforcement stiffness. For the analyses that consider the effective parameters for the backfill soil (Figure 7) and those considering total parameters (Figure 8), there are reductions in horizontal displacements with the use of stiffer reinforcements.

Similar to the considerations made for the magnitude of the maximum tension in the reinforcements (since there is no significant difference between the heavy and light compaction in the analyses with the use of total parameters), the horizontal displacements of the face are very close for this condition.

For the analyses using the effective parameters of the backfill soil, there is a significant difference between the analyses with heavy compaction closest to the face ($a = 0$ m and $a = 0.25$ m) and those that use heavy compaction farthest from the face ($a = 0.50$ m and $a = 1.00$ m). For the condition where $a = 0.25$ m and $a = 0.50$ m, especially for the upper layers of the reinforcements, there are smaller displacements, compared with the ones observed in the bottom layers of the GRSW. The higher the stiffness of the reinforcement leads to smaller displacements of the upper layers in the analyses with heavy compaction closest to the face ($a = 0$ m and $a = 0.25$ m).

The vertical induced stress generated by compaction, $\sigma'_{zc,i}$ and the horizontal induced stress, $\sigma'_{xp,i}$ ($\sigma'_{xp,i} = K_o \cdot \sigma'_{zc,i}$), are greater than the geostatic vertical and horizontal stresses ($\sigma'_h = K_a \cdot \sigma'_v$). So, according to Ehrlich & Mitchell (1994), the geosynthetic is submitted to a transitory high level of stress with a portion of unrecovered stress, as measured by Riccio et al. (2014).

However, this displacement is opposed to lateral pressures due to the compaction of the backfill. In this way, when carrying out the analyses with increasing distance of heavy compaction from the face, consequently with reducing the portion of reinforcements subjected to the loads of this

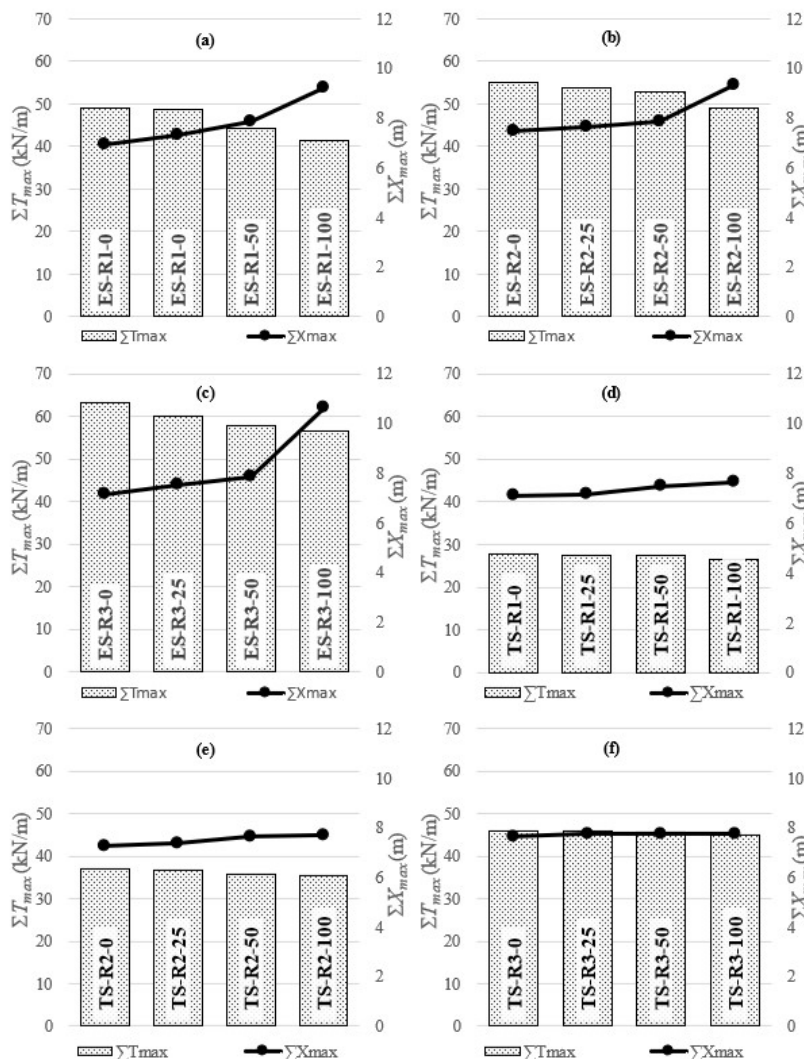


Figure 4. Influence of the stiffness modulus of the reinforcement (J) and the distance of heavy compaction from the face on the sum of the magnitude of the maximum tensions in the reinforcements (ΣT_{max}) and on the sum of the positions at which the maximum tensions in the reinforcements occur (ΣX_{max}).

compaction, there is a point where the maximum horizontal displacements occur. For the analyses performed, this maximum displacement occurred with 0.50 m distance of heavy compaction from the face.

In both analyses, the horizontal displacements of lower layers of the reinforcements are restricted by the stiffness of the foundation. In fact, according to Bathurst et al. (2009), the tensions in the reinforcements may be higher the half-height of the wall, generating larger deformations in this region. Another observation refers to the point where the maximum horizontal displacements (U_x) occur. In the analyses with the application of heavy compaction closest to the face ($a = 0$ m and $a = 0.25$ m), the points at which the maximum horizontal displacements occur are approximately half the height of the walls. In those that use heavy compaction farthest from the face ($a = 0.50$ m and $a = 1.00$ m), these points are elevated;

however, these displacements are not maximum at the top of the structure.

Importantly, in executing GRSW, the analysis with the application of heavy compaction nearest to the face ($a = 0$ m and $a = 0.25$ m) is difficult to perform. Thus, the analyses that considered heavy compaction farthest from the face ($a = 0.50$ m and $a = 1.00$ m) are more consistent with the conditions found in the real works. For the latter, as can be seen in Figure 7 and Figure 8, by moving the application of heavy compaction away from the face, face displacements were reduced.

Note that the results obtained numerically for the face horizontal displacements show similarities with other results found in the literature Miyata (1996), Helwany et al. (1999), Reeves (2003), Farrag et al. (2004), Yoo & Jung (2004), Benjamim et al. (2007), Bathurst et al. (2009) and Yang et al. (2009). The pattern

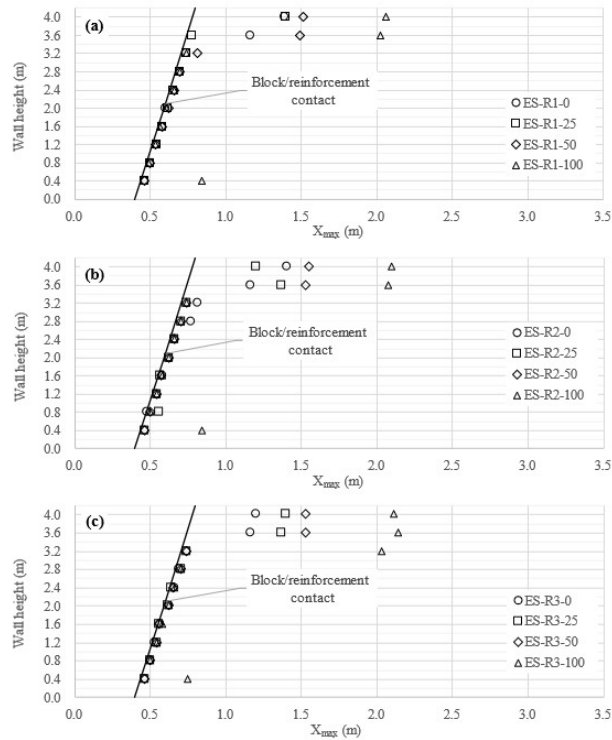


Figure 5. Positions of the maximum tensions in the reinforcements (X_{max}): numerical analyses in terms of Effective Stress (ES) when considering reinforcement stiffness (J) equal to (a) 400 kPa, (b) 800 kPa and (c) 1500 kPa.

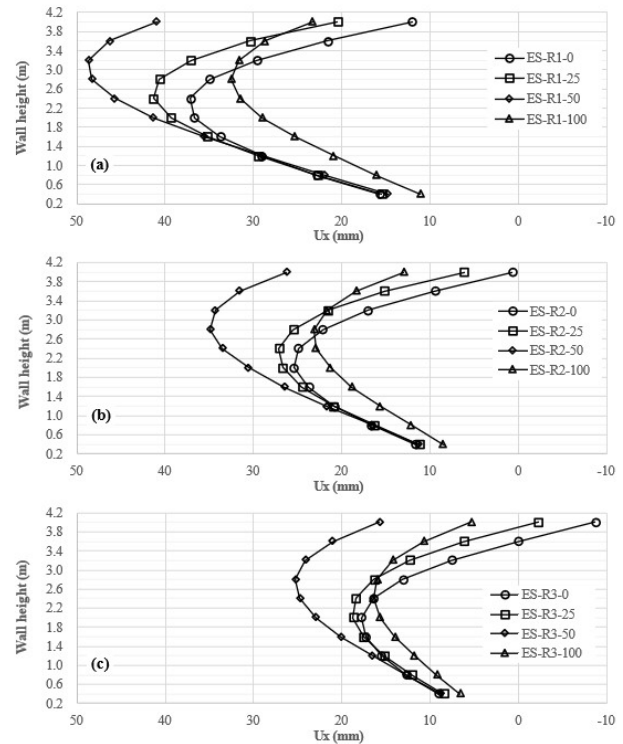


Figure 7. Horizontal displacements of the face: analyses in terms of effective stress (ES), considering the reinforcement stiffness (J) equal to (a) 400 kPa, (b) 800 kPa and (c) 1500 kPa.

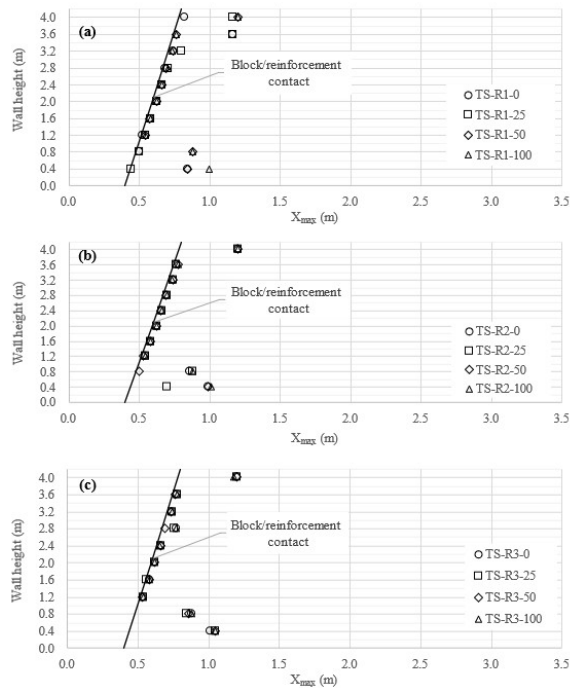


Figure 6. Positions of the maximum tensions in the reinforcements (X_{max}): numerical analyses in terms of Total Stress (TS) when considering reinforcement stiffness (J) equal to (a) 400 kPa, (b) 800 kPa and (c) 1500 kPa.

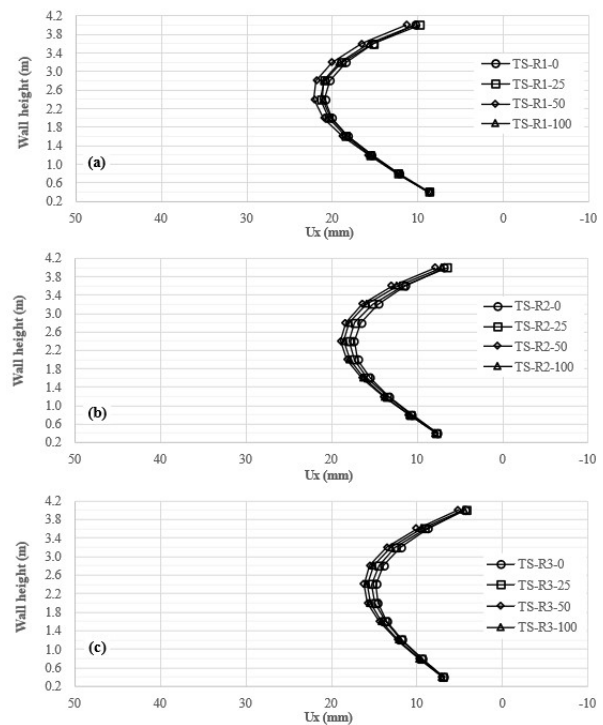


Figure 8. Horizontal displacements of the face: analyses in terms of total stress (TS), considering the reinforcement stiffness (J) equal to (a) 400 kPa, (b) 800 kPa and (c) 1500 kPa.

found for the maximum horizontal displacements of the face was also identified in the field measurements presented by Reeves (2003), with maximum deformations in the half-height portion of the GRSW. The data measured by Reeves (2003) were used by several authors to validate numerical models or design methods. The field measurements presented by Reeves (2003) were made on walls of soil reinforced with steel mesh, an enveloped face and light compaction.

Farrag et al. (2004) and Benjamim et al. (2007) also presented data on displacements of the face of reinforced soil walls built in full scale. They observed the same pattern found by Reeves (2003), i.e., maximum displacements at the half-height of the wall. However, it should be noted that in Farrag et al. (2004), although the wall was built with geogrids, as reinforcement elements, and concrete face blocks, there is no information on the type soil compaction used (light or heavy compaction). In Benjamim et al. (2007), the GRSW was built using an enveloped face, geotextiles, as reinforcement elements, and light compaction to densify the soil.

However, Riccio et al. (2014) found in an instrumented GRSW, locations of T_{max} not close to the face along the depth of the wall. The monitored GRSW had similar characteristics to the hypothetical GRSW presented in this study, but the foundation of the retaining wall monitored by Riccio et al. (2014) was a piled concrete slab.

3. Conclusions

This study presents a computational model of a GRSW using soil shear strength parameters obtained from triaxial tests. The objective was to analyse the influence of compaction in the magnitude of the tensions in the reinforcements, face horizontal deformation and position of maximum reinforcement's tension. The main conclusions are as follows.

In general, the results show the importance of considering the compaction-induced effects. In the analyses performed, the compaction caused influence on the magnitude and position of the maximum tensions in the reinforcements and the horizontal displacements of the face were determined. It is also identified that, with increasing stiffness of the reinforcements, there is an increase in the tensions mobilized and a reduction in the horizontal displacements of the face.

When analysing the influence of using distances close to the face for applying light compaction, it was identified that, by increasing these distances, that is, by moving the heavy compaction away from the face, there is a reduction in the sum of maximum tensions in the reinforcements ($\sum T_{max}$) and an increase in the sum of the positions at which T_{max} ($\sum X_{max}$) occurs. The increase in the positions at which T_{max} occurs means greater distances of T_{max} in relation to the face with increasing distance of heavy compaction from the face, especially for the upper layers. This increasing distance of T_{max} from the face is an important aspect to analyse since it will imply a reduction of the lengths of reinforcements in the resistant zone and, consequently, reduction in the factor of safety to pull-out.

Concerning the horizontal displacements of the face, it was expected that when distancing the heavy compaction from the face, there would be reductions in the displacements of the face. This behaviour was identified in the analyses in which the light compaction was considered in the first 0.50 m and 1.00 m behind the face. However, for the analyses in which only the application of heavy compaction was considered or the application of light compaction in the first 0.25 m behind the face was considered, the face displacements were smaller, especially in the upper portion of the walls analysed. It is understood that this behaviour may be associated with some factors, such as:

- Consideration of a 0.40 m wide drainage layer behind the face. Thus, for the analyses where the distance of heavy compaction was zero or 0.25 m, heavy compaction is supported on stiffer materials;
- Reducing the vertical stress induced by compaction in the region close to the face reduces the stiffness of the materials in the region since, with the use of the Hardening Soil model, the stiffness is a function of the confining stress;
- The linear elastic behaviour of the reinforcement and the perfect adhesion of the reinforcement with the soil. In this way, a greater extension of loads referring to the heavy compaction causes greater unloading and return of the elements to the original position.

It should be noted that the analyses considering heavy compaction at the face or a distance of only 0.25 m do not adequately represent the actual conditions of the work since in practice it is difficult to perform heavy compaction at distances less than 0.50 m from the face. Thus, when considering the analyses that are more consistent with the conditions of the constructive practices, that is, distances of 0.50 m and 1.00 m, it was observed that by moving the heavy compaction away from the face, there is a reduction of the sum of maximum tensions in the reinforcements, displacement towards the interior of the soil mass of the points at which the maximum tensions occur and reduction in horizontal displacements of the face. The results indicate that, mainly for the numerical evaluation of face displacements (U_x) and position of the maximum tension in the reinforcements (X_{max}), one should avoid the application of the vertical stress induced by compaction close to the face of GRSW in compaction modelling as in the analyses using zero or 0.25 m spacing.

It is important to highlight that the results obtained are limited to the considerations adopted for the analyses, such as soil type, reinforcement elements, face, foundation conditions and loads corresponding to the stresses induced by compaction.

Acknowledgements

The authors thank CNPq (Brazilian Council of Research), FAPEMIG (Minas Gerais State Council of Research) and CAPES (Coordination for the Improvement of Higher Education Personnel).

Declaration of interest

The authors have no conflicts of interest to declare. All co-authors have observed and affirmed the contents of the paper and there is no financial interest to report.

Authors' contributions

Leone César Meireles: conceptualization, investigation, data curation, formal analysis, writing – original draft, writing – review and editing. Mario Vicente Riccio Filho: conceptualization, investigation, data curation, formal analysis, writing – review and editing. Heraldo Nunes Pitanga: conceptualization, investigation, data curation, formal analysis, writing – review and editing. Roberto Lopes Ferraz: conceptualization, investigation, data curation, formal analysis, writing – review and editing. Taciano Oliveira da Silva: conceptualization, investigation, data curation, formal analysis, writing – review and editing. Sérgio Leandro Scher Dias Neto: conceptualization, investigation, data curation, formal analysis, writing – review and editing.

List of symbols

a	heavy compaction distance from the face
c	cohesion intercept
c'	effective cohesion intercept
E	Young modulus
E_i	initial stiffness
E_{ur}	unloading/reloading stiffness
E_{50}^{ref}	stiffnesses of the material for the reference confining tension in loading
E_{eod}^{ref}	modulus obtained from oedometric test
E_{ur}^{ref}	stiffnesses of the material for the reference confining tension in unloading and reloading
J	stiffness of reinforcement
K	hyperbolic parameter
K_a	active earth pressure coefficient
K_0	coefficient of earth pressure at rest
m	exponential coefficient
p^{ref}	reference confining tension
q_c	distributed load
R_{inter}	interface friction factor
T_{max}	maximum tension in the reinforcement
U_x	horizontal displacements
X	positions at which the maximum tensions occur
Z	depth
γ	unit weight
ν	poisson Coefficient
ϕ	friction angle (°)
ϕ'	effective friction angle (°)
φ	effective diameter of soil particles
ΣT_{max}	sum of the maximum tensions acting on the reinforcements

ΣX_{max}	sum of the positions at which the maximum tensions occur
σ_3	consolidation stresses
σ'_h	effective horizontal stress
σ'_v	effective vertical stress
$\sigma_{xp,i}$	horizontal stress induced by compaction
$\sigma_{zc,i}$	vertical stress induced by compaction
ψ	dilatancy angle

References

- ASTM D4767. (2011). *Standard Test Method for Consolidated Undrained Triaxial Compression Test for Cohesive Soils*. ASTM International, West Conshohocken, PA.
- ASTM D2487-17. (2017). *Standard Practice for Classification of Soils for Engineering Purposes (Unified Soil Classification System)*. ASTM International, West Conshohocken, PA.
- Bathurst, R.J., & Ezzein, F.M. (2016). Geogrid pullout load–strain behaviour and modelling using a transparent granular soil. *Geosynthetics International*, 23(4), 271-286. <http://dx.doi.org/10.1680/jgein.15.00051>.
- Bathurst, R.J., Nernheim, A., Walters, D.L., Allen, T.M., Burgess, P., & Saunders, D.D. (2009). Influence of reinforcement stiffness and compaction on the performance of four geosynthetic-reinforced soil walls. *Geosynthetics International*, 16(1), 43-59. <http://dx.doi.org/10.1680/jgein.2009.16.1.43>.
- Benjamin, C.V.S., Bueno, B.S., & Zornberg, J.G. (2007). Field monitoring evaluation of geotextile-reinforced soil-retaining walls. *Geosynthetics International*, 14(2), 100-118. <http://dx.doi.org/10.1680/jgein.2007.14.2.100>.
- Brinkgreve, R., & Vermeer, P. (2002). *PLAXIS 2D: Finite Element Code for Soil and Rock Analyses - Version 8*. CRC Press.
- Chen, J., Zhang, W., & Xue, J. (2017). Zoning of reinforcement forces in geosynthetic reinforced cohesionless soil slopes. *Geosynthetics International*, 24(6), 565-574. <http://dx.doi.org/10.1680/jgein.17.00023>.
- Christopher, B.R., Gill, S.A., Giroud, J.P., Juran, I., Mitchell, J.K., Schlosser, F., & Dunnycliff, J. (1990). *Reinforced soil structures* (Vol. 1: Design and Construction Guidelines). U.S. Department of Transportation, Federal Highway Administration.
- Duncan, J.M., Bryne, P., Wong, K.S., & Mabrt, P. (1980). *Strength, stress-strain and bulk modulus parameters for finite element analyses of stresses and movements in soil masses*. College of Engineering, Office of Research Services, University of California.
- Dyer, M.R., & Milligan, G.W. (1984). A photoelastic investigation of the interaction of a cohesionless soil with reinforcement placed at different orientations. In *Proceedings of the International Conference on In Situ Soil and Rock Reinforcement* (pp. 257-262). Paris: ISSMFE.
- Ehrlich, M., & Mirmoradi, S.H. (2013). Evaluation of the effects of facing stiffness and toe resistance on the behavior

- of GRS walls. *Geotextiles and Geomembranes*, 40, 28-36. <http://dx.doi.org/10.1016/j.geotexmem.2013.07.012>.
- Ehrlich, M., & Mirmoradi, S.H. (2016). A simplified working stress design method for reinforced soil walls. *Geotechnique*, 66(10), 854-863. <http://dx.doi.org/10.1680/jgeot.16.P.010>.
- Ehrlich, M., & Mitchell, J. K. (1994). Working stress design method for reinforced soil walls. *Journal of Geotechnical Engineering*, 120(4), 625-645. [http://dx.doi.org/10.1061/\(ASCE\)0733-9410\(1994\)120:4\(625\)](http://dx.doi.org/10.1061/(ASCE)0733-9410(1994)120:4(625)).
- Ehrlich, M., Mirmoradi, S.H., & Saramago, R.P. (2012). Evaluation of the effect of compaction on the behavior of geosynthetic-reinforced soil walls. *Geotextiles and Geomembranes*, 34, 108-115. <http://dx.doi.org/10.1016/j.geotexmem.2012.05.005>.
- Elias, V., Christopher, B. R., & Berg, R. R. (2001). *Mechanically stabilized earth walls and reinforced soil slopes – design and construction guidelines* [No. FHWA-NHI-00-043]. U.S. Department of Transportation, Federal Highway Administration.
- Farrag, K., Abu-Farsakh, M., & Morvant, M. (2004). Stress and strain monitoring of reinforced soil test wall. *Transportation Research Record: Journal of the Transportation Research Board*, 1868(1), 89-99. <http://dx.doi.org/10.3141/1868-10>.
- Hatami, K., & Bathurst, R.J. (2005). Development and verification of a numerical model for the analysis of geosynthetic-reinforced soil segmental walls under working stress conditions. *Canadian Geotechnical Journal*, 42(4), 1066-1085.
- Hatami, K., Witthoef, A.F., & Jenkins, L.M. (2008). Influence of inadequate compaction near facing on construction response of wrapped-face mechanically stabilized earth walls. *Transportation Research Record: Journal of the Transportation Research Board*, 2045(1), 85-94. <http://dx.doi.org/10.3141/2045-10>.
- Helwany, S.M.B., Reardon, G., & Wu, J.T.H. (1999). Effects of backfill on the performance of GRS retaining walls. *Geotextiles and Geomembranes*, 17(1), 1-16. [http://dx.doi.org/10.1016/S0266-1144\(98\)00021-1](http://dx.doi.org/10.1016/S0266-1144(98)00021-1).
- Jewell, R.A. (1980). *Some effects of reinforcement on the mechanical behavior of soils*. University of Cambridge.
- Koerner, R.M., & Koerner, G.R. (2018). An extended data base and recommendations regarding 320 failed geosynthetic reinforced mechanically stabilized earth (MSE) walls. *Geotextiles and Geomembranes*, 46(6), 904-912. <http://dx.doi.org/10.1016/j.geotexmem.2018.07.013>.
- Mirmoradi, S.H. (2015). *Evaluation of the behavior of reinforced soil walls under working stress conditions* [Doctoral thesis]. Federal University of Rio de Janeiro. Retrieved in October 28, 2022, from <http://www.coc.ufrj.br/en/doctoral-thesis/584-2015/5336-seyedhamed-mirmoradi>.
- Mirmoradi, S.H., & Ehrlich, M. (2014). Modeling of the compaction-induced stresses in numerical analyses of grs walls. *International Journal of Computational Methods*, 11(2), 1342002. <http://dx.doi.org/10.1142/S0219876213420024>.
- Mirmoradi, S.H., & Ehrlich, M. (2018a). Numerical simulation of compaction-induced stress for the analysis of RS walls under working conditions. *Geotextiles and Geomembranes*, 46(3), 354-365. <http://dx.doi.org/10.1016/j.geotexmem.2018.01.006>.
- Mirmoradi, S.H., & Ehrlich, M. (2018b). Experimental evaluation of the effect of compaction near facing on the behavior of GRS walls. *Geotextiles and Geomembranes*, 46(5), 566-574. <http://dx.doi.org/10.1016/j.geotexmem.2018.04.010>.
- Mirmoradi, S.H., Ehrlich, M., & Dieguez, C. (2016). Evaluation of the combined effect of toe resistance and facing inclination on the behavior of GRS walls. *Geotextiles and Geomembranes*, 44(3), 287-294. <http://dx.doi.org/10.1016/j.geotexmem.2015.12.003>.
- Mitchell, J. K., & Villter, W. B. (1987). *Reinforcement of earth slopes and embankments*. National Academies of Sciences, Engineering, and Medicine.
- Miyata, K. (1996). Walls reinforced with fiber reinforced plastic geogrids in Japan. *Geosynthetics International*, 3(1), 1-11. <http://dx.doi.org/10.1680/gein.3.0050>.
- Mohamad, G., Lourenço, P.B., & Roman, H.R. (2007). Mechanics of hollow concrete block masonry prisms under compression: review and prospects. *Cement and Concrete Composites*, 29(3), 181-192. <http://dx.doi.org/10.1016/j.cemconcomp.2006.11.003>.
- Reeves, J.W. (2003). *Performance of a full-scale wrapped face welded wire mesh reinforced soil retaining wall* [Master thesis]. Royal Military College of Canada (RMC).
- Riccio, M., Ehrlich, M., & Dias, D. (2014). Field monitoring and analyses of the response of a block-faced geogrid wall using fine-grained tropical soils. *Geotextiles and Geomembranes*, 42(2), 127-138. <http://dx.doi.org/10.1016/j.geotexmem.2014.01.006>.
- Saramago, R. P. (2002). *Study of the influence of compaction on the behavior of reinforced soil walls using physical models* [Doctoral thesis]. Federal University of Rio de Janeiro. (in Portuguese). Retrieved in October 28, 2022, from <http://www.coc.ufrj.br/pt/teses-de-doutorado/146-2002/926-robson-palhas-saramago>
- Yang, G., Zhang, B., Lv, P., & Zhou, Q. (2009). Behaviour of geogrid reinforced soil retaining wall with concrete-rigid facing. *Geotextiles and Geomembranes*, 27(5), 350-356. <http://dx.doi.org/10.1016/j.geotexmem.2009.03.001>.
- Yoo, C., & Jung, H.-S. (2004). Measured behavior of a geosynthetic-reinforced segmental retaining wall in a tiered configuration. *Geotextiles and Geomembranes*, 22(5), 359-376. [http://dx.doi.org/10.1016/S0266-1144\(03\)00064-5](http://dx.doi.org/10.1016/S0266-1144(03)00064-5).